Pisias, N.G., Mayer, L.A., Janecek, T.R., Palmer-Julson, A., and van Andel, T.H. (Eds.), 1995
Proceedings of the Ocean Drilling Program, Scientific Results, Vol. 138

41. STRONTIUM ISOTOPES IN PORE WATERS OF EAST EQUATORIAL PACIFIC SEDIMENTS: INDICATORS OF SEAWATER ADVECTION THROUGH OCEANIC CRUST AND SEDIMENTS[1]

S. Oyun,[2] H. Elderfield,[2] and G.P. Klinkhammer[3]

ABSTRACT

Pore-water samples from the equatorial sedimentary bulge area show reversals in depth profiles of $^{87}Sr/^{86}Sr$ ratios at the sediment/basement interface. Results of this work support inferences made from previous pore-water data (from DSDP drilling in the area) that large-scale horizontal advection of seawater has occurred through the basement underlying the thick sedimentary sequence in this region. The area of apparent advection includes the eastern part of the equatorial high-productivity zone and part of the Guatemala Basin. We attempted to find links between the observed near-basement reversals in pore-water chemistry and sedimentary thickness, age, and topography of the area. Most of the sites that show horizontal advection have disturbed basement topography or outcrops within 10 to 20 km, suggesting that the cooling effects of outcrops may extend for at least 20 km horizontally. Heat-flow data from the area were compared to determine whether sites showing near-bottom chemistry reversals were consistent with areas of low conductive heat flow. This was generally true for the area of the sedimentary bulge and Guatemala Basin. Not enough pore-water data from the Nazca Plate were available to establish any reliable systematics. Because the high-productivity area is well-sealed from hydrothermal circulation, the missing heat must be lost by horizontal advective heat transport. From profiles of strontium isotopes and other elements that show departure from seawater values with increasing depth in the sediments, but return to seawater values near the basement, it appears that water flows relatively freely through much of the oceanic crust, even when sealed by considerable sedimentary cover.

INTRODUCTION

Oceanic heat-flow measurements performed during the last few decades show large scatter over relatively small areas of the ocean floor (Anderson et al., 1976; Anderson and Langseth, 1977; Langseth and Anderson, 1979; Sclater et al., 1980). At mid-ocean spreading centers, hydrothermal circulation carries heat and geochemical fluxes to the open ocean through hydrothermal vents (Edmond et al., 1979). In ridge flanks, circulation continues at lower temperatures and rates of flow. Open circulation of water between the ocean crust and the sea is thought to cease where the sediment cover becomes complete; in these areas, the mean observed heat flow is usually in good agreement with the theoretical one.

However, a significantly different flow regime was identified recently by Baker et al. (1991) from work on pore waters from Deep Sea Drilling Project (DSDP) cores recovered in the equatorial Pacific. The area (105°–160°W, 5°–8°N) is coincident with the sedimentary bulge resulting from equatorial high productivity throughout the Cenozoic (Hey et al., 1972). Temporally, the area is about 10 to 70 Ma distant from the Pacific Ocean spreading centers. Furthermore, rapid sedimentation has created a nearly ubiquitous sedimentary cover up to several hundred meters thick (Hey et al., 1972). As a consequence, the vigorous hydrothermal convection characteristic of young oceanic ridges would be expected to have ceased, and the measured heat flows should represent reliable conductive values. Nevertheless, previous studies (Sclater et al., 1976) had shown that the area is characterized by anomalously low heat flow, about 50% to 67% of model predictions based on a conductively cooling lithosphere.

Measurements performed by Baker et al. (1991) of the profiles of Sr isotopic compositions of pore waters from DSDP Sites 572, 573, and 574 were found to show reversals at depth such that $^{87}Sr/^{86}Sr$ ratios trend toward present-day values for seawater as basement is approached. This demonstrated that there must be large-scale horizontal advection of young, cold seawater through the permeable basement underlying this thick sedimentary cover. This advection can account for the anomalously low heat-flow characteristic of the area.

In this preliminary report, extensive data sets of Sr concentrations and Sr isotopic compositions of pore waters from all Leg 138 sites are presented that cover the Cocos, Nazca, and Pacific plates. This is used to test the hypothesis of lateral flow of unaltered seawater through the basaltic basement and to chart its possible extent.

METHODS

Sites drilled during Leg 138 are located on three lithospheric plates of the equatorial Pacific: the Cocos, Nazca, and Pacific plates (Fig. 1 and Table 1). The sediments recovered were primarily biogenous, and the region is remote from terrestrial sources of clastic sediments and from shallow areas supplying neritic sediments. Furthermore, the sediments contain only a few thin ash layers. Pore-water samples from all 11 sites were obtained for strontium isotopic analysis.

Pore waters were extracted using a stainless-steel, Manheim-type squeezer (Sayles et al., 1973) at room temperature and filtered through 0.45 mm Gelman acrodisk disposable filters before shipboard analysis and storage of samples for shore-based analysis. The details of the shipboard procedures are summarized in the Leg 138 *Initial Reports* volume (Mayer, Pisias, Janecek, et al., 1992), where the results of the shipboard analytical program also are listed.

Pore-water samples for strontium (Sr) isotopic analysis were heat-sealed in plastic tubing after extraction and were transported to Cambridge for analysis. We selected 58 pore-water samples for analysis on the basis of depth below the seafloor and the shapes of profiles for other pore-water species. Sr was separated from 100 µL aliquots by conventional cation exchange chromatography, and $^{87}Sr/^{86}Sr$ ratios were determined using a VG Sector 54 instrument having 7 collectors using a multidynamic peak switching program. Individual mean measurements (10 sets of 10) were performed for each sample to ensure that no biasing was introduced into the data. Each mass was collected over a time interval of 5 s, followed by a 2-s gap, which ensures that no bias was present in the peak heights. The standard rejection was 3% of the data, and the σ rejection level was 2.5. The isotopic value recorded after rejection was usually taken as the final value. Results

[1] Pisias, N.G., Mayer, L.A., Janecek, T.R., Palmer-Julson, A., and van Andel, T.H. (Eds.), 1995. *Proc. ODP, Sci. Results*, 138: College Station, TX (Ocean Drilling Program).
[2] Department of Earth Sciences, University of Cambridge, Downing Street, Cambridge CB2 3EQ, United Kingdom.
[3] College of Oceanography, Oregon State University, Corvallis, OR 97331-5503, U.S.A.

Table 1. Summary of Leg 138 sites and Sr-isotope reversals.

Site	Location	Longitude (°W)	Latitude (°N)	Age (Ma)	Sedimentary cover (m)	Depth drilled (mbsf)	Sedimentation rates (m/m.y.)	Heat flow of the area	Local topography	$^{87}Sr/^{86}Sr$ profile near basement
844	Guatemala Basin	90°28′	7°55′	17.5	300	290.8	30–35	Low	Topography minimal, seamount 8 km SW, 475m above seafloor	Reversal
845	Guatemala Basin	94°35′	9°34′	17	291	291.6	25–40	Low	Topography minimal, rough basement, no outcrops	Reversal
846	South of Galapagos Islands	90°49′	3°05′S	16.5	422	422.4	20–50	High	Flat and undisturbed, no outcrops	No reversal[a]
847	West of Galapagos Islands	95°19′	0°11′	7	295	231.0	30–80	High	Topographic high, relatively rough basement	Basement not reached
848	EEP, sed. bulge	110°28′	2°59′S	11	93.3	93.3	10–20	Low	Number of small peaks and troughs, rough basement	Reversal
849	EEP, sed. bulge	110°31′	0°10′N	10.5	350	350.5	20–100	Low	A small outcrop 10–15 km W, 300 m above seafloor	Reversal
850	EEP, sed. bulge	110°31′	1°17′	12	399	399.8	20–100	low	A topographic high, with rough basement, outcrop 9 km S	Reversal
851	EEP, sed. bulge	110°34′	2°46′	11	320	320.5	30–70	Low	Topographic high, with complex basement relief	Reversal
852	EEP, sed. bulge	110°4′	5°17′	10	125	117.3	10–25	Low	Topographic high, with rough basement relief	Reversal
853	West of EPR	109°45′	7°12′	7	73	72.4	5–15	High	Small topographic high, no outcrops	No reversal
854	West of EPR	109°35′	11°13′	9	46	46.0	2–15	High	No major topographic features	No reversal

Notes: In the "Sedimentary Cover" column, there are no major differences in the lithostratigraphy at all sites, and the presence of volcanic ash is negligible. EEP = East Equatorial Pacific, and EPR = East Pacific Rise.

[a] Reversal in Sr^{2+} (see Fig. 2).

obtained for NBS 987 $SrCO_3$ standard during the course of the research gave $^{87}Sr/^{86}Sr = 0.710251$, and samples of an in-house seawater standard gave $^{87}Sr/^{86}Sr = 0.70917$.

The complete set of $^{87}Sr/^{86}Sr$ ratios for the pore-water samples is given in Table 2 and illustrated as profiles in Figure 2, alongside profiles of Sr^{2+} concentrations. The principal characteristic of the profiles (whether they exhibited near-basement reversals) also is noted in Table 1.

RESULTS

The overall range of Sr-isotope ratios in pore waters from Leg 138 is from 0.708942 to 0.709177. The average $^{87}Sr/^{86}Sr$ ratio near the sediment/seawater interface for all sites is 0.709165, which agrees with the modern seawater value of 0.70917.

All sites except Site 847, in which chert layers were encountered 50 m above the basaltic crust, were drilled to the basement. From those, pore-water samples from all sites of the equatorial high productivity zone (Sites 848–852) show near-bottom reversals in Sr isotopes and Sr^{2+} (Fig. 2) and also Li^+, SO_4^{2-}, and alkalinity (Mayer, Pisias, Janecek, et al., 1992). Dissolved Ca^{2+} and Mg^{2+} profiles at these sites are rather flat (Mayer, Pisias, Janecek, et al., 1992). Sites 853 and 854, which are not part of the equatorial high productivity zone, do not show near-bottom reversals. Sites 844 and 845 on the Cocos Plate also show reversals in Sr-isotope and other pore-water profiles. Site 846 on the Nazca Plate does not show the near-bottom reversal in the Sr-isotope profile, but does show it in other chemical species.

DISCUSSION

Behavior of Strontium in Carbonate Sediments

At any time, the isotopic composition of dissolved Sr in the oceans is uniform, because the oceanic residence time of Sr (ca. 2 Ma) greatly exceeds the oceanic mixing time (ca. 10^3 yr). The concentration of Sr in today's ocean is about 90 μM, and the $^{87}Sr/^{86}Sr$ ratio is 0.70917. Over the course of geological time, the Sr-isotope ratio has changed because of changes in the fluxes of Sr from various isotopically different sources (Elderfield, 1986).

When deep-ocean carbonate sediments are deposited, they preserve, subject to diagenesis, the contemporaneous seawater $^{87}Sr/^{86}Sr$ value, which reflects all the main fluxes. The data of Burke et al. (1982) show that a rapid monotonic increase in $^{87}Sr/^{86}Sr$ in seawater occurred during most parts of the Cenozoic. Therefore, $^{87}Sr/^{86}Sr$ ratios of pore waters of oceanic sediments should, and in general do (Elderfield and Gieskes, 1982), decrease with increasing depth. The original $^{87}Sr/^{86}Sr$ ratio is further influenced by diagenetic reactions in the sedimentary column (see Elderfield and Gieskes, 1982; Gieskes et al., 1986; Richter and DePaolo, 1987, 1988). As a consequence of carbonate diagenesis, Sr^{2+} concentrations in pore waters increase with depth because the distribution coefficient (D_{Sr}) for biogenic calcite is ~0.16, whereas that for inorganic equilibrium calcite precipitation is 0.044 (Katz et al., 1972; Lorens, 1981; Baker et al., 1982). The diagenetic return flux of Sr from deep-sea carbonate oozes acts as a partial buffer to temporal isotopic change (Elderfield and Gieskes, 1982; F.M. Richter and Y. Liang, unpubl. data, 1993). Thus, $^{87}Sr/^{86}Sr$ ratios in marine sedimentary pore waters depart from both modern and contemporaneous seawater values with increasing depth downcore.

Evidence for Fluid Flow

Away from oceanic ridge systems, as oceanic crust ages and cools, and basalts are buried by a sufficiently thick and continuous sedimentary cover, the pore-water system becomes closed to most chemical and isotopic exchanges with the ocean. Diffusion through the sediments dominates advection or reaction for most constituents. In these cases, the $^{87}Sr/^{86}Sr$ profiles would be expected to show the features outlined above, accompanied by heat-flow values near the theoretical

ones for conductive cooling. However, like the DSDP sites identified by Baker et al. (1991), all of the Leg 138 sites, with two or possibly three exceptions, show reversals in $^{87}Sr/^{86}Sr$ ratios and Sr^{2+} concentrations in pore waters near basement (Fig. 2). The exceptions are Sites 853, 854, and possibly 846 (there is a significant reversal for Sr^{2+}, not obvious for $^{87}Sr/^{86}Sr$ ratios).

The $^{87}Sr/^{86}Sr$ ratios and Sr^{2+} concentrations in the pore waters nearest the basement are shown in Table 3 and are compared with values for modern seawater and of $^{87}Sr/^{86}Sr$ ratios of seawater of the age of the basement. Excluding the sites having no reversals and Site 847 where near-basement pore waters were not sampled, the average $^{87}Sr/^{86}Sr$ ratio of the pore waters nearest the basement is 0.70910, near the value of 0.70917 for modern seawater. In contrast, the calculated $^{87}Sr/^{86}Sr$ ratios for contemporaneous seawater fall in the range of 0.70860 to 0.70885. The equivalent average value for Sr^{2+} in the near-basement pore waters is 98 μM, similar to 90 μM in seawater. This is overwhelming evidence for the presence of modern seawater in the upper part of the oceanic crust at these sites.

Thus, the results of this study support the proposal of Baker et al. (1991) that large-scale lateral advection of seawater occurs through oceanic crust in the equatorial Pacific Ocean. The study of Baker et al. (1991) was based on three sites in the equatorial Pacific sediment bulge to the west of East Pacific Rise. This study is based on a further five sites in this area (Sites 848–852). In addition, we show evidence for fluid flow in the Guatemala Basin to the east of the ridge (Sites 844 and 845).

Leg 138 Sites 853 and 854 do not exhibit reversals. The sedimentary cover at these sites is very thin (65 and 45 m, respectively); as discussed below, this is the likely reason for their contrasting behavior to the other sites.

Factors Affecting Pore-water Profiles

In Table 1, we compare the sedimentary thickness, age, sedimentary rates, and topography of the Leg 138 sites, factors that might be expected to affect the pore-water profiles.

Sedimentary Thickness

A sediment thickness of about 100 to 150 m seems necessary to seal the vertical advection of seawater throughout the whole of the sediment column (McDuff, 1981). This depends upon the temperature of the basement as well as sediment type and sedimentation rate. Sites 853 and 854, both of which have a thin sedimentary cover, indicate the least-extreme profiles and the most radiogenic Sr-isotope values from those sites with approximately the same ages, but thicker sedimentary covers. This indicates that sedimentary thickness, rather than age, controls the advection. With increasing sedimentary cover, the Sr-isotope profiles become more extreme (Fig. 2). All sites showing near-bottom reversals are at least 100 m thick. The exception is Site 846, which has the thickest sediment cover but no reversal. However, the $^{87}Sr/^{86}Sr$ ratios at Site 846 depart strongly from the contemporaneous seawater values as basement is approached and the profiles of other chemical elements, such as Sr^{2+} (Fig. 2), Li^+, SO_4^{2-} and alkalinity (Mayer, Pisias, Janecek, et al., 1992), all show clear near-bottom reversals at this site. Therefore, the data from Site 846 can also be interpreted in terms of fluid flow.

Local Topography

Near most of the sites that exhibit evidence of horizontal water advection, the basement topography is rough and disturbed and basement outcrops lie within 10 to 15 km of three of them. These outcrops might serve as sites of recharge of fresh, cold seawater, which then flows horizontally and discharges at other basement seamounts or tectonic zones. In spite of their relatively high porosity, sediments are generally several orders of magnitude less permeable than the basalts they cover. When oceanic basement is buried by a sufficiently thick and continuous sedimentary cover, the system becomes closed to most chemical and isotopic exchanges with the ocean. Diffusion through the sediments dominates advection or reaction. Lister (1970) suggested that where areas of "permeable" oceanic crust outcrop through sediment, most of the heat would be lost by mass transport through the outcrops. This loss of heat should give rise to the low heat-flow values that often are observed in the sediments surrounding these outcrops.

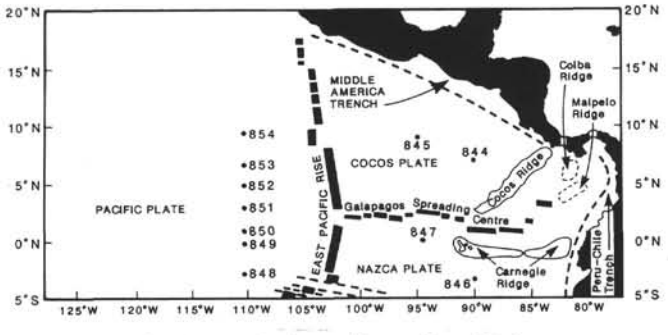

Figure 1. Map of study area showing positions of Leg 138 sites.

Heat Flow

Heat-flow data from the study area were compared to determine whether sites exhibiting near-bottom reversals were consistent with areas of low conductive heat flow relative to theoretically predicted heat flow (Fig. 3). This was generally true for the western transect of Leg 138 (Sites 848–852) and sites at Guatemala Basin (844 and 845). These sites are situated in low heat-flow areas first identified by Von Herzen and Uyeda (1963). In contrast, Sites 853 and 854 are located within the area of higher heat flow and do not possess Sr-isotope reversals. Heat-flow data at the Nazca Plate are scattered, and not enough pore-water data are available to establish any reliable systematics. Because the high-productivity area is well sealed to hydrothermal circulation, the missing heat must be lost by horizontal advective heat transport, with the heat-carrying seawater being ventilated through basaltic outcrops.

Evidence from Other ODP/DSDP Sites in the Eastern Pacific Ocean

Pore-water data from other East Pacific sites drilled previously have been compiled (Fig. 3). Supporting evidence for large-scale horizontal advection of water in the equatorial high-productivity area comes from Sites 572, 573, 574, 66, 69, 73, 77, 79, 81, and 82. However, a number of sites either were not drilled to the basement, or they lack the chemical information based upon the recovered cores. Therefore, it is difficult to conclude whether the whole of the area of the equatorial sedimentary bulge exhibits large-scale water advection at the sediment/basalt interface. It is apparent, however, that the horizontal advection is a broad-scale regional phenomenon for, at least, most of the eastern part of the high-productivity zone.

Fluid Flow Within Sediments

Comparison of Sr-isotope profiles with contemporaneous seawater curves are also shown in Figure 2. The contemporaneous seawater curves were constructed for each site using the age equations derived from a reference seawater curve (Ohde and Elderfield, 1992). At all sites, the pore waters are distinctly more radiogenic than contemporaneous seawater. Diagenetic effects usually result in small shifts in $^{87}Sr/^{86}Sr$ ratio, the maximum difference being on the order of 5×10^{-5} (Richter and DePaolo, 1987, 1988). A comparison of the

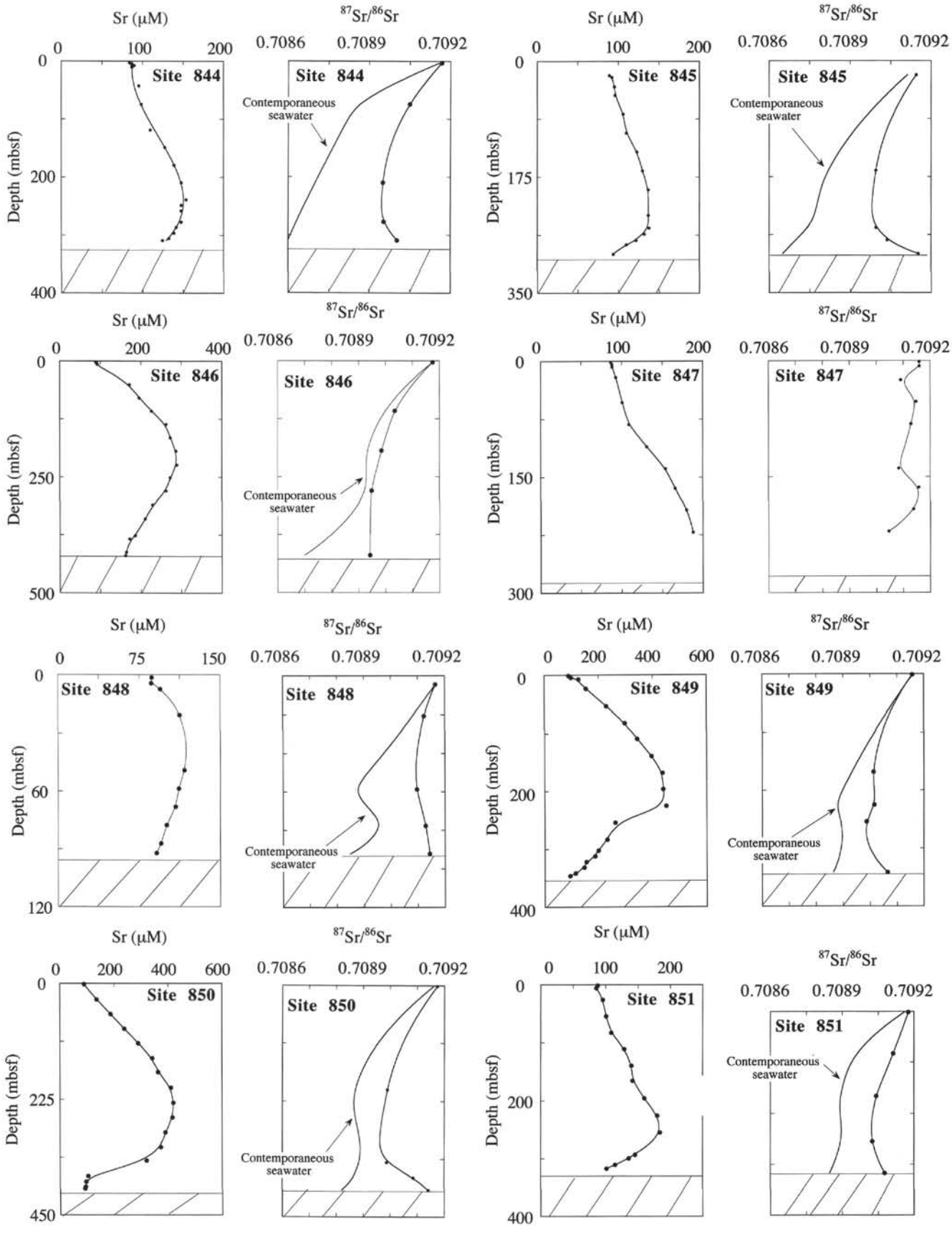

Figure 2. Depth profiles of Sr concentrations and $^{87}Sr/^{86}Sr$ ratios for Leg 138 sites. The shaded area represents the oceanic basement. Also shown are the Sr-isotope curves for seawater vs. time for each site except Site 847 (basement was not sampled at this site).

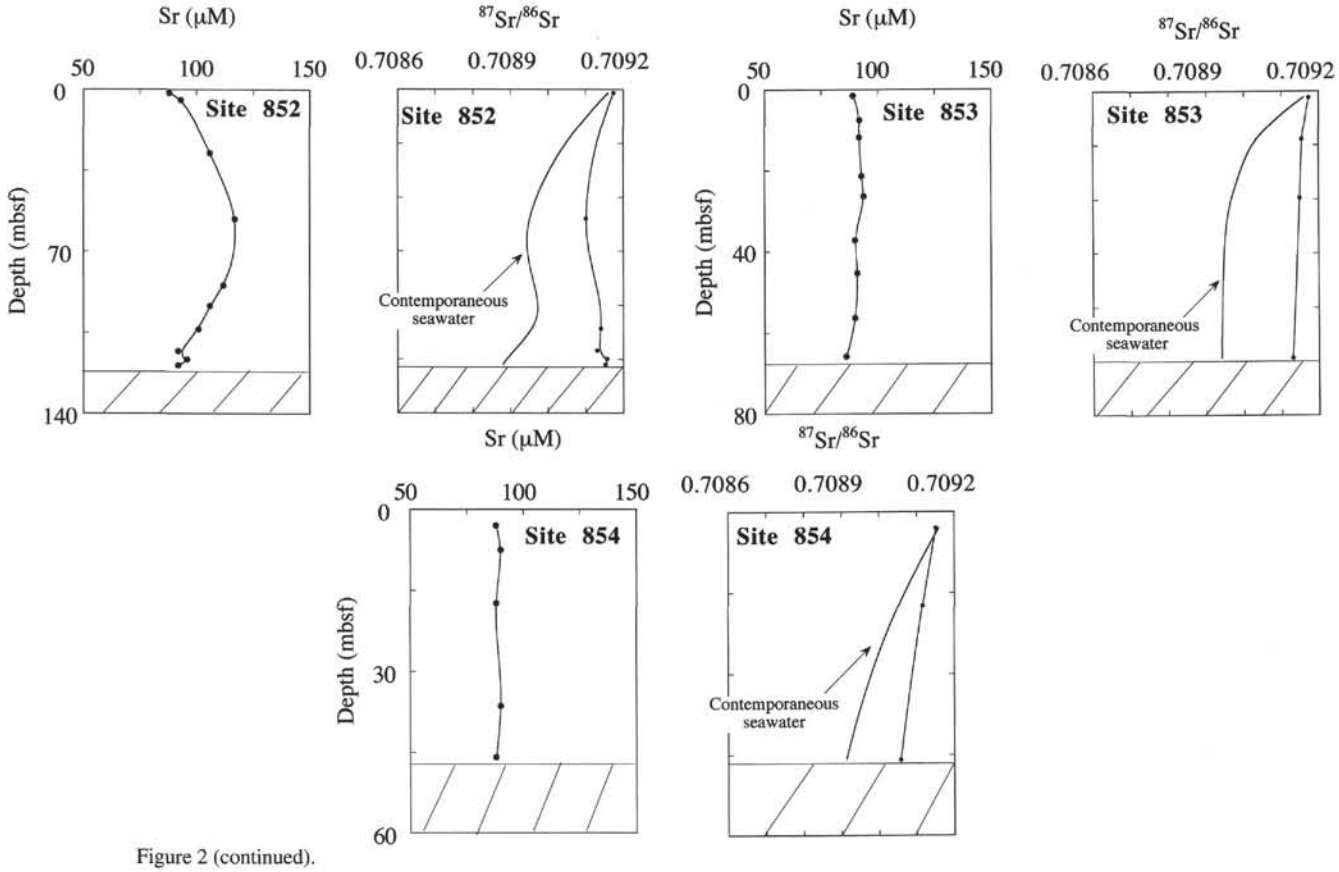

Figure 2 (continued).

contemporaneous seawater curve with the minimum $^{87}Sr/^{86}Sr$ values at each site shows differences from 9×10^{-5} to 30×10^{-5}, shifts two to six times larger than can be accounted for by the above diagenetic models. However, application of diagenetic models to these particular sites is needed before the Sr-isotope shifts can be assumed to be anomalous. Because the area is distant from any significant influence from Sr of continental origin, the more radiogenic Sr profiles, if confirmed, may indicate upward flow of seawater from the horizontally advecting seawater within the upper crust. Recently, Richter (1993) modeled the Sr-isotope data of Baker et al. (1991) to estimate the vertical component of fluid flow. It will be important to consider this approach to the area as a whole using the results from this study.

SUMMARY

Data of the concentrations and isotopic compositions of Sr are presented for 53 samples representing all Leg 138 sites. All profiles at Sites 844, 845, 846, 848, 849, 850, 851, and 852 show near-basement reversals to near-modern seawater values. This demonstrates that fluid flow occurs within the upper oceanic crust in the region of the equatorial Pacific sediment bulge and in the Guatemala Basin. Basement was not reached at Site 847. Sites 853 and 854 do not show reversals, which has been attributed to the thin sediment cover. A comparison of Sr-isotope profiles with contemporaneous seawater values suggests that fluid flow within the sediment pile may be occurring as a consequence of the basement flow.

ACKNOWLEDGMENTS

We are grateful to the staff of ODP, both on and off the *JOIDES Resolution* for their support of this work. We thank Mervyn Greaves and Ann Williams for invaluable laboratory assistance. Paul Baker, Andy Fisher, and Miriam Kastner provided helpful reviews of the manuscript. This work was supported by NERC Grant GR3/7828

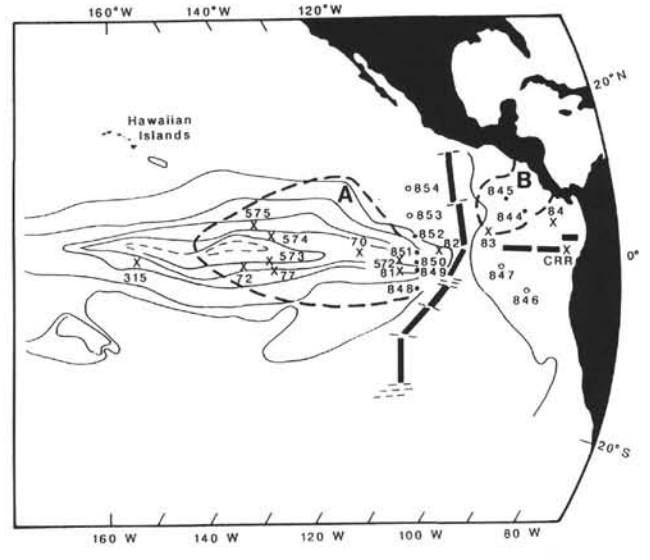

Figure 3. Locations of Eastern Equatorial Pacific Ocean sites showing supporting evidence for large-scale lateral advection and areas of low heat-flow values in the region. Closed symbols = Leg 138 sites having near-basement reversals. Open symbols = Leg 138 sites having no reversals. Crosses = other ODP/DSDP Sites in the area showing supporting evidence for seawater advection. The shaded areas are those of anomalously low heat flow in the area: A = equatorial sediment bulge; B = Guatemala Basin. Heat-flow data from Von Herzen and Uyeda (1963), Langseth et al. (1965), Lee and Uyeda (1965), McKenzie and Sclater (1967), Anderson et al. (1976), Sclater et al. (1976), and Stein and Abbot (1991). Isopachs of sediment thickness are in 10^2 m (Ewing et al., 1968).

Table 2. $^{87}Sr/^{86}Sr$ ratios and Sr concentrations of Leg 138 pore waters.

Core section, interval (cm)	Depth (mbsf)	Sr (μM)	$^{87}Sr/^{86}Sr$ ($\pm 10^{6} \bullet 2\sigma$)
138-844A-			
1H-1, 145–150	2.9	84.1	0.709168 (24)
1H-2, 145–150	4.4	87.0	—
1H-3, 145–150	5.9	87.0	—
1H-4, 145–150	7.4	89.9	—
1H-5, 145–150	8.9	87.0	—
1H-6, 145–150	10.4	87.0	—
138-844B-			
6H-4, 145–150	42.6	95.7	—
9H-4, 145–150	74.6	98.6	0.709050 (24)
12H-4, 145–150	119.0	110	—
15H-4, 145–150	149.0	128	—
18H-4, 145–150	179.5	139	—
21X-4, 145–150	209.6	148	0.708951 (26)
24X-4, 142–150	238.5	154	—
25X-4, 142–150	248.2	148	—
26X-4, 142–150	257.9	148	—
28X-4, 142–150	277.2	148	0.708954 (28)
29X-4, 142–150	286.5	142	—
30X-4, 142–150	296.5	139	—
31X-4, 142–150	305.8	133	—
38X-7, 46–54	309.3	125	0.709004 (30)
138-845C-			
1H-1, 147–150	21.5	89.1	0.709145 (26)
1H-3, 146–150	24.5	92.0	—
2H-6, 145–150	38.9	95.2	—
138-845A-			
6H-4, 145–150	51.6	96.1	—
9H-4, 145–150	80.1	106	—
12H-4, 145–150	108.6	110	—
15H-4, 145–150	137.1	123	—
18H-4, 145–150	165.6	130	0.708995 (26)
21X-4, 145–150	194.1	137	—
25X-4, 145–150	232.5	137	—
27X-4, 142–150	251.8	138	0.708996 (24)
28X-4, 142–150	261.0	132	—
29X-4, 147–150	270.6	122	0.709037 (26)
30X-2, 142–150	277.2	110	—
31X-5, 142–150	291.4	94.0	0.709153 (26)
138-846A-			
1H-2, 0–5		3.0	89
1H-3, 145–150	4.5	91	—
1H-5, 0–5	7.5	93	—
6H-4, 145–150	51.0	172	—
9H-4, 145–150	79.5	196	—
12H-4, 145–150	108.0	227	0.709035 (28)
15H-4, 145–150	136.5	263	—
18H-4, 145–150	165.0	273	—
21H-4, 145–150	193.5	287	0.708986 (28)
24X-5, 145–150	223.7	289	—
27X-4, 140–150	251.2	273	—
30X-4, 140–150	279.9	263	0.708949 (28)
33X-5, 140–150	310.3	229	—
36X-6, 140–150	340.7	210	—
40X-4, 140–150	376.3	186	—
41X-4, 140–150	383.9	172	—
44X-3, 80–92	412.5	164	—
45X-1, 10–15	419.6	162	0.708942 (28)
138-847A-			
1H-1, 145–150	1.5	86.9	0.709159 (24)
1H-3, 135–140	4.4	88.2	—
1H-5, 135–140	7.4	88.3	0.709160 (24)
138-847B-			
3H-6, 145–150	21.0	93.0	0.709091 (24)
6H-6, 145–150	53.5	101	0.709147 (24)
9H-6, 145–150	82.0	109	0.709129 (22)
12H-6, 145–150	110.5	131	—
15H-6, 145–150	139.0	154	0.709084 (26)
18X-6, 145–150	164.5	166	0.709158 (24)
21X-6, 145–150	192.5	180	0.709138 (26)
24X-6, 145–150	221.5	188	0.709046 (26)
138-848A-			
1H-1, 145–150	1.5	86.9	—
1H-3, 145–150	4.5	86.5	0.709166 (24)
1H-5, 145–150	7.5	94.8	—
138-848B-			
3H-6, 145–150	20.7	112.7	0.709124 (26)
6H-6, 145–150	49.2	116.9	—
7H-6, 145–150	58.7	111.7	0.709097 (32)
8H-6, 145–150	68.2	108.7	—
9H-6, 145–150	77.7	100.5	0.709129 (26)
10H-6, 145–150	87.2	95.2	—
11H-3, 145–150	92.2	91.0	0.709144 (30)
138-849A-			
1H-1, 145–150	1.5	90	0.709158 (28)
1H-3, 145–150	4.5	99	—
1H-5, 145–150	7.5	127	—
138-849B-			
3H-5, 145–150	23.7	155	—
6H-6, 145–150	53.7	230	—
9H-6, 145–150	82.2	298	—
12H-5, 145–150	109.2	343	—
15X-6, 145–150	139.3	396	—
18X-6, 142–150	168.3	436	0.709013 (28)
21X-6, 144–150	196.3	439	—
24X-6, 144–150	225.3	450	0.709016 (22)
27X-6, 144–150	254.3	262	0.708987 (24)
30X-6, 144–150	283.3	232	—
32X-6, 144–150	302.6	199	—
33X-6, 142–150	312.2	187	—
34X-6, 142–150	321.9	155	—
35X-6, 142–150	331.6	147	—
36X-6, 142–150	341.6	114	0.709065 (44)
37X-3, 142–150	346.3	94.0	—
138-850A-			
1H-1, 145–150	1.5	89	0.709174 (28)
138-850B-			
3H-6, 145–150	31.0	136	—
6H-6, 145–150	59.5	187	—
9H-6, 142–150	88.0	238	—
12X-6, 142–150	116.5	290	—
15X-6, 144–150	145.4	342	—
18X-5, 144–150	172.5	363	—
21X-6, 144–150	202.5	411	0.708990 (24)
24X-6, 144–150	231.5	420	—
27X-6, 145–150	260.0	417	—
30X-6, 144–150	288.9	390	—
33X-6, 142–150	317.9	373	—
36X-6, 140–150	343.8	320	0.708987 (22)
39X-6, 140–150	374.3	104	0.709086 (28)
40X-6, 140–150	385.4	97	—
41X-6, 140–150	395.1	95	—
42X-2, 140–150	398.8	92	0.709141 (24)
138-851A-			
1H-1, 135–140	1.4	88	0.709177 (26)
1H-4, 135–140	5.9	86	—
138-851B-			
3H-6, 145–150	26.0	96	—
6H-6, 145–150	54.5	101	—
9H-6, 145–150	83.0	109	0.709113 (28)
12H-6, 145–150	111.5	129	—
15H-6, 145–150	140.0	140	—
18X-4, 145–150	165.8	142	0.709042 (26)
21X-5, 142–150	195.8	160	—
24X-6, 142–150	225.8	180	—
27X-6, 142–150	254.8	184	0.709026 (28)
31X-6, 144–150	293.0	146	—
32X-4, 142–150	299.6	136	—
33X-5, 142–150	310.7	115	—
34X-3, 142–150	317.4	102	0.709078 (24)
138-852A-			
1H-1, 145–150	1.5	88	0.709174 (26)
1H-3, 145–150	4.5	93	—
138-852B-			
3H-6, 145–150	27.4	106	—
6H-6, 145–150	55.9	117	0.709101 (28)
9H-6, 145–150	84.4	112	—
10H-6, 145–150	93.3	106	—
11H-6, 145–150	103.4	101	0.709141 (28)
12H-4, 145–150	112.9	92	0.709131 (24)
138-852C-			
13X-4, 145–150	116.5	96	0.709157 (26)
13X-4, 96–104	119.0	92	0.709153 (26)
138-853A-			
1H-1, 141–150	1.5	89	0.709174 (26)
1H-5, 145–150	7.5	92	—
138-853B-			

Table 2 (continued).

Core section, interval (cm)	Depth (mbsf)	Sr (μM)	$^{87}Sr/^{86}Sr$ ($\pm 10^{6} \bullet 2\sigma$)
2H-5, 145–150	11.8	92	0.709155 (28)
3H-6, 145–150	21.3	93	—
4H-6, 145–150	26.3	94	0.709149 (28)
5H-6, 135–150	37.2	90	—
6H-6, 145–150	45.3	91	—
7H-6, 145–150	56.3	90	—
8H-6, 145–150	65.8	86	0.709130 (26)
138-854B-			
1H-2, 145–150	3.0	88	0.709152 (20)
1H-5, 145–150	7.5	90	—
2H-6, 145–150	17.4	88	0.709116 (24)
4H-6, 145–150	36.4	90	—
5H-6, 145–150	45.9	88	0.709058 (32)

Table 3. $^{87}Sr/^{86}Sr$ ratios and Sr concentrations in pore waters nearest to basement compared with values for modern seawater and seawater of basement age.

Site	Age (Ma)	$^{87}Sr/^{86}Sr$ ratio: Measured nearest to basement	$^{87}Sr/^{86}Sr$ ratio: Seawater of basement age	Sr measured nearest to basement (μM)
844	17.5	0.70900	0.70860	125
845	17	0.70915	0.70865	94
846	17	0.70894	0.70870	162
847	7	0.70905	0.70894	188
848	11	0.70914	0.70885	91
849	10.5	0.70907	0.70886	94
850	11–12	0.70914	0.70882	92
851	11	0.70908	0.70885	102
852	10	0.70915	0.70888	92
853	7–10	0.70913	0.70894	86
854	9–10	0.70906	0.70891	88
Average		0.70910		98 μM
Modern seawater		0.70916		90 μM

(H.E.) and a Research Studentship from The British Council BC-MON/2234 to S.O. This is Cambridge Earth Sciences Series Contribution No. 3369.

REFERENCES*

Anderson, R.N., Langseth, M.G., and Sclater, J.G., 1977. The mechanisms of heat transfer through the floor of the Indian Ocean. *J. Geophys. Res.*, 82:3391–3409.

Anderson, R.N., Langseth, M.G., Vacquier, V., and Francheteau, J., 1976. New terrestrial heat flow measurements on the Nazca plate. *Earth Planet. Sci. Lett.*, 29:243–354.

Baker, P.A., Gieskes, J.M., and Elderfield, H., 1982. Diagenesis of carbonates in deep-sea sediments: evidence from Sr^{2+}/Ca^{2+} ratios and interstitial dissolved Sr^{2+} data. *J. Sediment. Petrol.*, 52:71–82.

Baker, P.A., Stout, P.M., Kastner, M., and Elderfield, H., 1991. Large-scale lateral advection of seawater through oceanic crust in the central equatorial Pacific. *Earth Planet. Sci. Lett.*, 105:522–533.

Burke, W.H., Denison, R.E., Hetherington, E.A., Koepnick, R.B., Nelson, H.F., and Otto, J.B., 1982. Variation of seawater $^{87}Sr/^{86}Sr$ throughout Phanerozoic time. *Geology*, 10:516–519.

Edmond, J.M., Measures, C., McDuff, R.E., Chan, L.H., Collier, R., and Grant, B., 1979. Ridge crest hydrothermal activity and the balances of the major and minor elements in the ocean. *Earth Planet. Sci. Lett.*, 46:1–18.

Elderfield, H., 1986. Strontium isotope stratigraphy. *Palaeogeogr., Palaeoclimatol., Palaeoecol.*, 57:71–90.

Elderfield, H., and Gieskes, J.M., 1982. Sr isotopes in interstitial waters of marine sediments from Deep Sea Drilling Project cores. *Nature*, 300:493–497.

Ewing, J., Ewing, M., Aitken, T., and Ludwig, W.J., 1968. North Pacific sediment layers measured by seismic profiling. *In* Knopoff, L., Drake, C.L., and Hart, P.J. (Eds.), *The Crust and Upper Mantle of the Pacific Area.* Am. Geophys. Union. Monogr., 12:147–173.

Gieskes, J.M., Elderfield, H., and Palmer, M.R., 1986. Strontium and its isotopic composition in interstitial waters of marine carbonate sediments. *Earth Planet. Sci. Lett.*, 77:229–235.

Hey, R., Leonard, G., and Lowrie, A., 1972. The Galapagos triple junction and plate motions in the Equatorial Pacific. *Nature*, 237:20–22.

Katz, A., Sass, E., Starinsky, A., and Holland, H.D., 1972. Strontium behavior in the aragonite-calcite transformation: an experimental study at 40°–98°. *Geochim. Cosmochim. Acta*, 36:481–496.

Langseth, M.G., and Anderson, R.N., 1979. Correction. *J. Geophys. Res.*, 84:1139–1140.

Langseth, M.G., Grim, P.J., and Ewing, M., 1965. Heat flow measurements in the East Pacific Ocean. *J. Geophys. Res.*, 70:367–380.

Lee, W.H.K., and Uyeda, S., 1965. Review of heat flow data. *Geophys. Monogr.*, 8:87–186.

Lister, C.R.B., 1970. Heat flow west of the Juan de Fuca Ridge. *J. Geophys. Res.*, 75:2648–2654.

Lorens, R.B., 1981. Sr, Cd, Mn and Co distribution coefficients in calcite as a function of calcite precipitation rate. *Geochim. Cosmochim. Acta.*, 45:553–561.

Mayer, L., Pisias, N., Janecek, T., et al., 1992. *Proc. ODP, Init. Repts.*, 138 (Pts. 1 and 2): College Station, TX (Ocean Drilling Program).

McDuff, R.E., 1981. Major cation gradients in DSDP interstitial waters: the role of diffusive exchange between seawater and upper ocean crust. *Geochim. Cosmochim. Acta*, 45:1705–1713.

McKenzie, D.P., and Sclater, J.G., 1967. Heat flow in the East Pacific and sea floor spreading. *Bull. Volcanol.*, 33:101–108.

Ohde, S., and Elderfield, H., 1992. Strontium isotope stratigraphy of Kita-Daito-Jima Atoll, North Philippine Sea: implications for Neogene sea-level change and tectonic history. *Earth Planet. Sci. Lett.*, 113:473–486.

Richter, F.M., 1993. Fluid flow in deep-sea carbonates: estimates based on porewater Sr. *Earth Planet. Sci. Lett.*, 119:133–141.

Richter, F.M., and DePaolo, D.J., 1987. Numerical models for diagenesis and the Neogene Sr isotopic evolution of seawater from DSDP Site 590B. *Earth Planet. Sci. Lett.*, 83:27–38.

————, 1988. Diagenesis and Sr isotope evolution of seawater using data from DSDP 590B and 575. *Earth Planet. Sci. Lett.*, 90:382–394.

Sayles, F.L., Manheim, F.T., and Waterman, L.S., 1973. Interstitial water studies on small core samples, Leg 15. *In* Heezen, B.C., MacGregor, I.D., et al., *Init. Repts. DSDP*, 20: Washington (U.S. Govt. Printing Office), 783–804.

Sclater, J.G., Crowe, J., and Anderson, R.N., 1976. On the reliability of ocean heat flow averages. *J. Geophys. Res.*, 81:2997–3006.

Sclater, J.G., Jaupart, C., and Galson, D., 1980. The heat flow through oceanic and continental crust and the heat loss of the Earth. *Rev. Geophys.*, 18:269–311.

Stein, C.A. and Abbot, D.A., 1991. Heat flow constraints on the South Pacific Superswell. *J. Geophys. Res.*, 96:16083–16099.

Von Herzen, R.P., and Uyeda, S., 1963. Heat flow through the Eastern Pacific Ocean floor. *J. Geophys. Res.*, 68:4219–4250.

* Abbreviations for names of organizations and publications in ODP reference lists follow the style given in *Chemical Abstracts Service Source Index* (published by American Chemical Society).

Date of initial receipt: 11 February 1993
Date of acceptance: 8 February 1994
Ms 138SR-156